Majority of Southern Ocean seasonal sea ice bloom net community production precedes total ice retreat

Shannon McClish[1] and Seth M Bushinsky[2]

[1]University of Hawaii at Manoa
[2]University of Hawaii at Mānoa

December 15, 2022

Abstract

The Southern Ocean Seasonal Sea Ice Zone (SSIZ) is characterized by the development of spring phytoplankton blooms following retreating sea ice. Until recently, assessing SSIZ bloom carbon export has been limited by a lack of under ice observations. Here, we relate the timing of phytoplankton growth to the drawdown of surface nutrients and sea ice cover and estimate spring bloom net community production (bNCP) using biogeochemical profiling float observations. The onset of biological production follows initial sea ice breakup with 64% of bNCP under partial sea ice cover. Estimates of bNCP range from <1 to >4 mol C m^{-2} $bloom^{-1}$, with earlier sea ice breakup associated with higher bNCP, and the highest bNCP where micronutrient supply is likely enhanced by topographic-driven mixing. These results indicate that satellite-derived export estimates will underestimate bNCP in the SSIZ and have implications for future carbon export in a changing Southern Ocean sea ice regime.

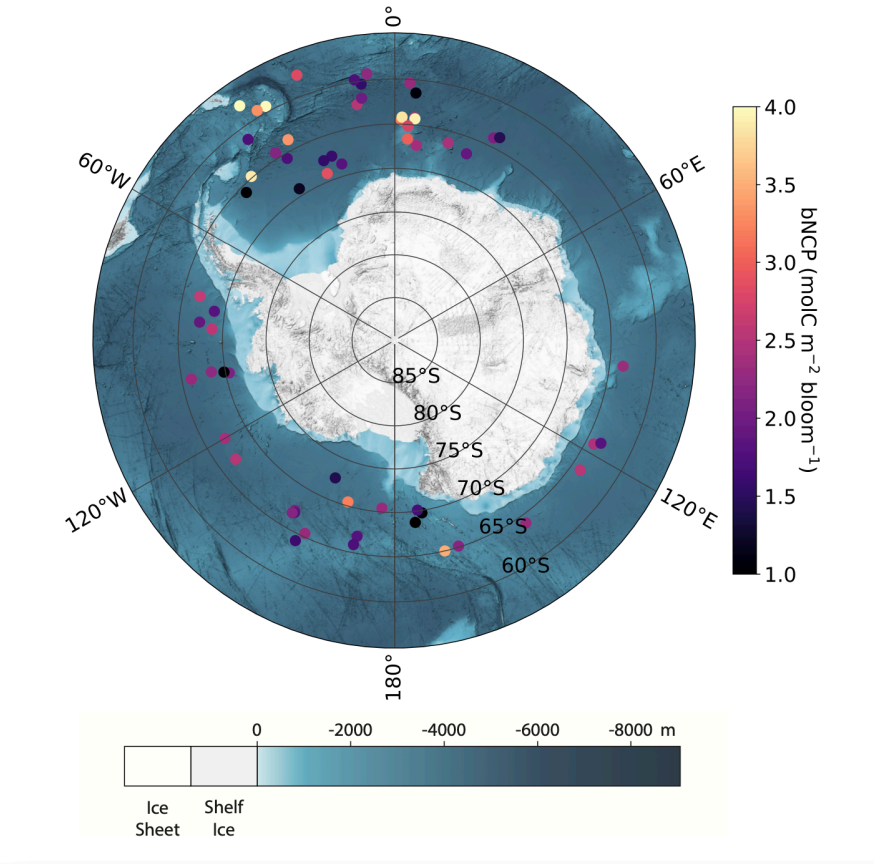

Figure 1: Mean float positions during spring bloom and associated net community 607 production. Ocean bathymetry (International Bathymetric chart of the Southern Ocean (IBSCO) 608 version 2(Dorschel et al., 2022) overlayed with circular markers indicating float positions during 609 spring nitrate minimum. Marker colors correspond to the magnitude of bNCP calculated from 610 integrated upper ocean nitrate changes during each spring bloom.

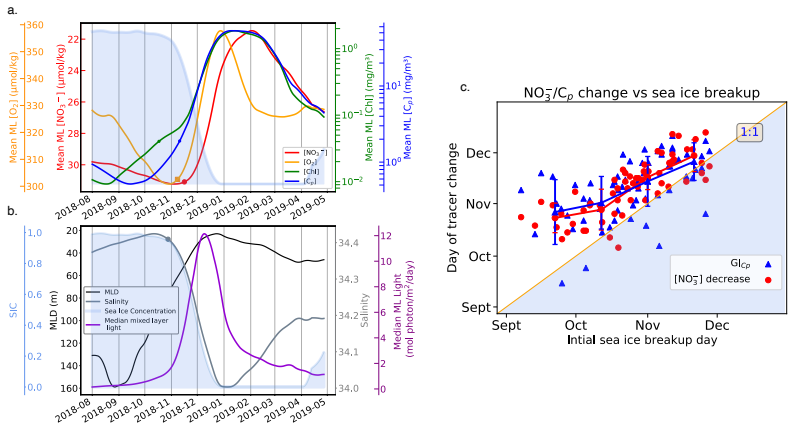

Figure 2: Figure 2. Seasonal relationships between mixed layer properties and sea ice. Example float 613 (WMO 5904471) winter to summer timeseries with mixed layer mean oxygen (orange), nitrate 614 (red), phytoplankton carbon (blue), and chlorophyll (green) concentrations (a.) and mixed layer 615 mean salinity, mixed layer depth, mixed layer median light (b.) with satellite SIC in shaded blue 616 for both (SIC scale on bottom panel only). Symbols indicate the day of GIChl,Cp or when nitrate, 617 oxygen, or salinity thresholds are exceeded. (c.) Relationships between date of sea ice breakup 618 relative to nitrate decrease and GICp date. The day of year of nitrate decrease (red circles) and GICp 619 (blue triangles) vs. sea ice breakup day for all 64 float seasons analyzed. Colored lines indicate 20- 620 day bin means ± 1 standard deviation. Symbols lying above the solid gold 1:1 line in the unshaded 621 region indicate mixed layer nitrate decrease and GICp after sea ice breakup

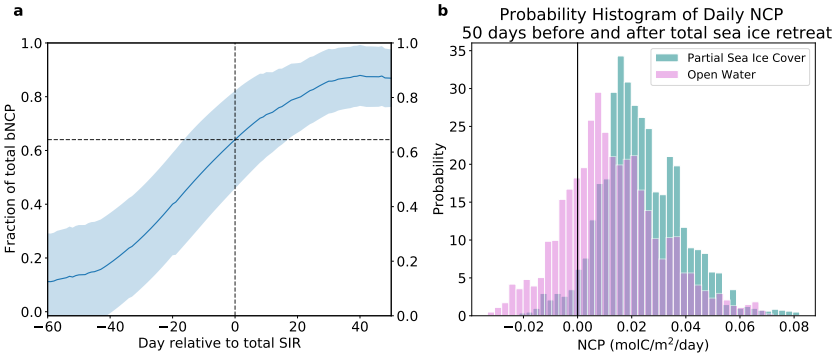

Figure 3: Figure 3. Relationship between calculated NCP and sea ice cover. a) Average cumulative 624 fraction of total bNCP for all floats (solid line) with respect to total sea ice retreat (dashed vertical line) and ± 1 std deviation (shaded region). b) Probability histogram of daily NCP rates 50 days 626 before (green) and 50 days after (pink) total sea ice retreat date.

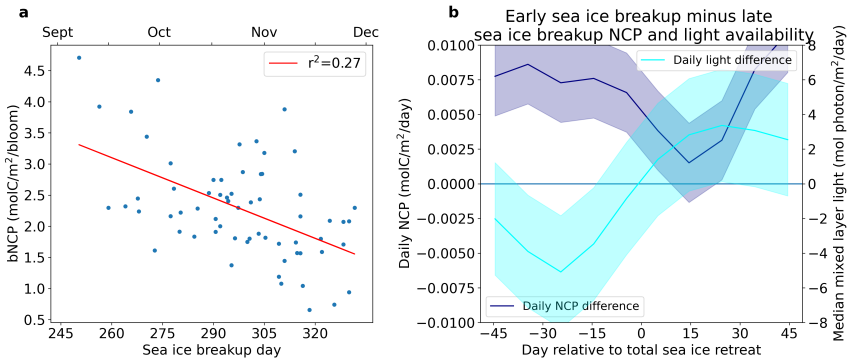

Figure 4: Figure 4. Relationship between NCP and timing of sea ice breakup. (a.) bNCP is negatively correlated (red line, P<.001) with date of sea ice breakup. (b.) Differences between 10-day binned mean daily NCP (purple line) and light availability (blue line) for early sea ice breakup and late sea ice breakup observations (before mid-October, day 290) minus late (after early November, day 310). Floats with observations of early sea ice breakup had higher daily NCP prior to total sea ice retreat despite lower light availability prior to total sea ice retreat.

Majority of Southern Ocean seasonal sea ice bloom net community production precedes total ice retreat

Shannon McClish* **and Seth M. Bushinsky**

Department of Oceanography, School of Ocean and Earth Science and Technology, University of Hawai‘i at Mānoa, Honolulu, HI

*Corresponding author, smcclish@hawaii.edu

Key points

- Majority of net community production during the Southern Ocean spring ice zone bloom occurs prior to full sea ice retreat
- Highest rates of daily net community production occur during active sea ice retreat and may be due to iron delivery or low grazing rates
- Highest observed bloom net community production is tied to early sea ice retreat and/or proximity to topographic features

Abstract

The Southern Ocean Seasonal Sea Ice Zone (SSIZ) is characterized by the development of spring phytoplankton blooms following retreating sea ice. Until recently, assessing SSIZ bloom carbon export has been limited by a lack of under ice observations. Here, we relate the timing of phytoplankton growth to the drawdown of surface nutrients and sea ice cover and estimate spring bloom net community production (bNCP) using biogeochemical profiling float observations. The onset of biological production follows initial sea ice breakup with 64% of bNCP under partial sea ice cover. Estimates of bNCP range from <1 to >4 mol C m^{-2} $bloom^{-1}$, with earlier sea ice breakup associated with higher bNCP, and the highest bNCP where micronutrient supply is likely enhanced by topographic-driven mixing. These results indicate that satellite-derived export estimates will underestimate bNCP in the SSIZ and have implications for future carbon export in a changing Southern Ocean sea ice regime.

Plain Language Summary

Sea ice around the Southern Ocean expands during the fall/winter and retreats each spring/summer. Massive spring blooms of phytoplankton are observed around the retreating sea ice edge, but observations of these blooms are limited by ice cover and difficult ocean conditions such that quantification of their biological impact has been difficult. In this study we use year-round data from profiling floats that measure oxygen, nitrate, chlorophyll fluorescence, and particulate backscatter. We use these data to determine that the spring phytoplankton bloom begins just after sea ice breaks up and the majority of organic matter that is produced but not consumed is generated before total sea ice retreat. This indicates that commonly used satellite observations miss most of the bloom period. We also found that the greatest organic matter production occurred in regions

of early sea ice retreat or near sea-floor features. We explored the potential role of phytoplankton growth limitation by micronutrients, such as iron, and consumption by grazing zooplankton, finding it likely that these drove the patterns of organic matter production seen in this study. These results indicate that changes in sea ice timing and magnitude due to climate change will likely impact biological production in the Southern Ocean.

Introduction

The Seasonal Sea Ice Zone (SSIZ) encompasses the roughly 16 million km^2 Southern Ocean region between the winter maximum and summer minimum sea ice extent. Winter sea ice formation inhibits light availability and air-sea gas exchange in the surface ocean and deepens the mixed layer through cooling and brine rejection. In spring, sea ice rapidly retreats and freshens the surface ocean, creating shallow mixed layers and increased light levels in surface waters. Elevated regions of chlorophyll identified in ocean color observations suggest phytoplankton blooms occur over a third of the SSIZ each spring (Fitch & Moore, 2007). The initiation of blooms in the SSIZ has been attributed to an increase in light levels, sea ice melt induced surface stratification, release of sea-ice algae, and/or increased iron supply from melting ice following sea ice retreat (Ardyna et al., 2017; Walker O. Smith & Comiso, 2008; Walker O. Smith & Nelson, 1985; Taylor et al., 2013a). However, a lack of under ice, multi-year, and basin wide observations has hindered a clear understanding of how sea ice impacts phytoplankton blooms and the associated nutrient and inorganic carbon drawdown. Recent record minima in Antarctic Sea ice extent and anomalously early sea ice retreats in 2017 and 2022 (Parkinson, 2019; Wang et al., 2022) underline the need to understand the link between sea ice retreat and biological processes in the Southern Ocean.

Estimates of net primary production (NPP) from satellite ocean color observations (Arrigo et al., 2008; Moore & Abbott, 2000), extrapolated from discrete sampling efforts (Buesseler et al., 2003; W. O. Smith & Nelson, 1986), and a biogeochemically coupled circulation model (Taylor et al., 2013b) find that the sea ice impacted Southern Ocean contributes between as little as 4% to as much as 15% of total Southern Ocean NPP. Estimates of NPP and prior research on bloom drivers in the SSIZ from ship surveys and satellite observations are constrained to the ice-free portion of the year. Recent deployment of profiling floats equipped with biogeochemical sensors, primarily by the Southern Ocean Carbon and Climate Observations and modeling project (Johnson, Plant, Coletti, et al., 2017), has enabled a more complete characterization of SSIZ blooms and associated NCP through under ice observations. Novel observations of chlorophyll fluorescence and particulate backscatter from biogeochemical profiling floats have provided new understanding of SSIZ bloom phenology, indicating that phytoplankton biomass begins to accumulate from September to October, prior to sea ice melt detection and several months prior to ice free conditions in January and February (L. A. Arteaga et al., 2020; Hague & Vichi, 2020; Horvat et al., 2022; Uchida et al., 2019).

However, the biogeochemical impact of SSIZ phytoplankton blooms on mixed layer carbon and nutrient cycling, especially during the under-ice season, and their broader role in the total Southern Ocean carbon cycle is unclear. Net community production (NCP) describes the fraction of primary production that is not respired at the surface and can be exported into the ocean interior. Prior estimates of NCP in the SSIZ are sparse in spatial and temporal extent and recent estimates from biogeochemical profiling floats using the seasonal change in mixed layer nitrate or mesopelagic oxygen concentration indicate a wide potential range in the magnitude of SSIZ NCP (1-3.5 mol C m^{-2} yr^{-1}) (L. A. Arteaga et al., 2019; von Berg et al., 2020; Johnson, Plant, Dunne, et

al., 2017). Here we link seasonal changes in phytoplankton biomass to NCP throughout the SSIZ from 2015-2021 to determine the link between sea ice breakup, nutrient drawdown and NCP.

Results

Timing of declining sea ice cover, phytoplankton biomass, and nutrient drawdown

We compare Southern Ocean Carbon and Climate Observation and Modeling float observations of salinity, nitrate, oxygen, float derived phytoplankton carbon (C_p), chlorophyll (Chl), and calculated mixed layer depth to along-track sea ice concentration and surface radiative flux. Data are from 31 floats, measuring 64 bloom periods from July 2015 to March 2021 (Fig. 1). We focus the analysis from July to March of each year, during which time mixed layer phytoplankton carbon, chlorophyll, and oxygen concentrations increase from their annual minima to maxima and mixed layer nitrate concentration and salinity decrease from annual maxima to minima (representative winter to summer period illustrated in Fig. 2). We use mixed layer mean values to investigate the order of events, which also allows close comparison with satellite-derived timing studies of surface ocean properties.

Changes in salinity, satellite SIC and an initial oxygen increase all can be used to independently identify the onset of sea ice melt and initial exposure of previously isolated water to atmospheric gases and increased light. We determine initial sea ice breakup timing using an average of these three proxies to minimize individual uncertainties. Total sea ice retreat is used to refer to the first day of sea ice free conditions and is determined from satellite SIC. We estimate growth initiation from both phytoplankton carbon (GI_{Cp}) and chlorophyll (GI_{Chl}) and compare these to the date of a decrease in mean mixed layer nitrate concentrations to identify the timing

between phytoplankton biomass increase from near zero values in peak winter and the draw down of surface nutrients and inorganic carbon due to biological growth.

Figure 2. Seasonal relationships between mixed layer properties and sea ice. Example float (WMO 5904471) winter to summer timeseries with mixed layer mean oxygen (orange), nitrate (red), phytoplankton carbon (blue), and chlorophyll (green) concentrations **(a.)** and mixed layer mean salinity, mixed layer depth, mixed layer median light **(b.)** with satellite SIC in shaded blue for both (SIC scale on bottom panel only). Symbols indicate the day of $GI_{Chl,Cp}$ or when nitrate, oxygen, or salinity thresholds are exceeded. **(c.)** Relationships between date of sea ice breakup relative to nitrate decrease and GI_{Cp} date. The day of year of nitrate decrease (red circles) and GI_{Cp} (blue triangles) vs. sea ice breakup day for all 64 float seasons analyzed. Colored lines indicate 20-day bin means ± 1 standard deviation. Symbols lying above the solid gold 1:1 line in the unshaded region indicate mixed layer nitrate decrease and GI_{Cp} after sea ice breakup.

The initial increase in mixed layer oxygen coincides with a decrease in mixed layer salinity and SIC, indicating sea ice breakup and invasion of atmospheric oxygen, and the onset of sea ice decrease (Fig. 2). The onset of sea ice breakup occurs 17 ± 12 days before the mixed layer nitrate decreases and 17 ± 18 days before growth initiation from phytoplankton carbon (GI_{Cp}) (Fig. 2c). GI_{Chl} occurs 7 ± 23 days before estimated sea ice breakup and does not show a consistent relationship with mixed layer nitrate decrease or growth initiation from phytoplankton carbon, though GI_{Chl} is almost always earlier. GI_{Chl} occurs 23 ± 23 days earlier than initial mixed layer nitrate decrease and 23 ± 21 days before GI_{Cp}. The longest delay between GI_{Chl} and GI_{Cp}/nitrate decrease is 76 and 80 days, respectively, which occurred early (~September), approximately two months before sea ice breakup (Fig. S2). While GI_{Cp} and mixed layer nitrate decrease almost always occur after initial sea ice breakup, the lag between sea ice breakup and GI_{Cp} and mixed layer nitrate decrease is greater earlier in the season (mid-September) than later (mid-November) (Fig. 2c).

147 *SSIZ bloom net community production*

148 NCP is calculated from nitrate drawdown down to the depth of the wintertime maximum
149 MLD to include production or respiration immediately beneath the mixed layer and in order to
150 determine the net transport of carbon from the surface ocean to depth, rather than redistribution of
151 carbon within the upper ocean that will be seasonally re-exposed to the atmosphere (Bushinsky &
152 Emerson, 2018; Johnson, Plant, Dunne, et al., 2017; Text S4). Daily NCP begins to be positive
153 coincident with mixed layer decreases in nitrate and increases in phytoplankton carbon (Fig. S3)
154 and continues to increase as the ice concentrations decline from near 100% sea ice concentration
155 to open water (Fig. 3a). On average 64% of the NCP associated with the seasonal sea ice zone
156 blooms, bloom NCP (bNCP), occurs under partial sea ice cover (Fig. 3a), and higher daily NCP is
157 observed prior to total sea ice retreat (Fig. 3b). Cumulative bNCP peaks between January and
158 April.

159

160 While observations of higher NCP between sea ice break up and total sea ice retreat are
161 consistent throughout all 64 float years, bNCP magnitude spanned a wide range of <1 to >4 mol
162 C m^{-2} $bloom^{-1}$. In order to identify possible drivers of the wide range in SSIZ bNCP, we test the
163 relationship between bNCP and timing of sea ice breakup, length of productive period (defined as
164 the period between minimum and maximum cumulative NCP), cumulative mixed layer depth
165 radiation adjusted for SIC, days with SIC < 15%, and duration of shallow mixed layers. Variability
166 in cumulative bNCP is related to the timing of sea ice breakup (r^2=0.27, *P*<.001), with higher
167 bNCP found when sea ice breakup occurs earlier, and lower bNCP when sea ice breakups later in
168 the year (Fig. 4). On average, bNCP is 1 mol C m^{-2} $bloom^{-1}$ higher in floats where sea ice retreat
169 begins on or before mid-October (day 290, 19 occurrences) than after early November (day 310,

20 occurrences). The higher bNCP with earlier breakup is not attributable to an increase duration of nitrate drawdown, as the duration of nitrate drawdown is only weakly linearly related to the magnitude of bNCP (r^2=.105, *P*=.009) (Fig. S4). Rather, the higher bNCP of floats which observe early sea ice retreat is associated with higher daily NCP rates, as well as higher mixed layer phytoplankton carbon concentrations following sea ice breakup (Fig. 4b, Fig. S5). Prior to total sea ice retreat, the floats that observe early sea ice breakup and higher daily NCP have lower light availability compared to observations with late sea ice breakup (Fig 4b).

Discussion

Biomass increases and NCP initiation

The onset of rapid phytoplankton biomass increase and nutrient drawdown occurs approximately two weeks after initial sea ice breakup (Fig. 2), suggesting that small openings in sea ice relieve light limitation and trigger biological production and associated biologically derived net community production in the SSIZ. Net autotrophy begins well before either total sea ice retreat or the 10-15% SIC contour commonly used to define the retreating sea ice edge in previous work assessing SSIZ blooms from ship surveys or satellite ocean color products (e.g., (Ardyna et al., 2017; Arrigo et al., 2008)). Onset of NCP following sea ice breakup is consistent with observations in the Arctic of increased phytoplankton biomass near leads and unconsolidated ice and correlations between chlorophyll, backscatter and sea ice thickness, and presence of leads in the Southern Ocean (Assmy et al., 2017; Bisson & Cael, 2021).

Our observed timing of growth initiation and the transition to net autotrophy confirms recent findings that production begins well prior to total sea ice retreat (L. A. Arteaga et al., 2020; Hague & Vichi, 2020; Horvat et al., 2022; Uchida et al., 2019). However, despite the increases in

193 chlorophyll observed weeks to months before initial sea ice breakup, we do not find any indication
194 of biological production sufficient to influence surface nutrient and carbon concentrations until
195 after sea ice breakup. Increases in chlorophyll (GI_{Chl}) prior to sea ice breakup are not concurrent
196 with GI_{Cp} or an observable decrease in nitrate (Fig. S2). The initial increases in chlorophyll
197 concentration are very small, and even when GI_{Chl} occurs months before sea ice opening, mixed
198 layer chlorophyll concentrations remain very low until sea ice breakup begins. The difference in
199 GI_{Cp} and GI_{Chl} timing are largely due to a high sensitivity of GI_{Chl} to very small changes in
200 chlorophyll concentration. If instead a 0.035 mg m^{-3} chlorophyll concentration threshold is used
201 based on the 0.2 μmol kg^{-1} nitrate concentration threshold and a chl:N ratio of 1.75 (Moreau et al.,
202 2020), growth initiation inferred from chlorophyll has a similar timing as both GI_{Cp} and nitrate
203 decrease (Fig. S2). The significant difference between identifying phytoplankton growth initiation
204 using the rate based GI_{Chl} or a chlorophyll concentration threshold based on meaningful
205 biogeochemical changes affects interpretation of drivers of phytoplankton growth, and indicates
206 the advantage of using backscatter and nitrate data in addition to chlorophyll to understand
207 seasonal changes in phytoplankton biomass in the SSIZ. This is especially true considering
208 inherent uncertainties involved in using chlorophyll fluorescence to estimate chlorophyll
209 concentrations and the near zero chlorophyll and phytoplankton concentrations in winter.

210 Previous hypotheses suggest that SSIZ blooms are stimulated by shallow mixed layers and
211 increased light following sea ice retreat. Our results suggest sea ice breakup, rather than near total
212 or total sea ice retreat, appears to relieve winter light limitation, even while SIC is still near the
213 winter maximum. During the remainder of the bloom period we do not find evidence for light as
214 the primary limiting factor affecting magnitude of total SSIZ bNCP. The cumulative available light
215 in the mixed layer, duration of ice-free days, or duration of shallow mixed layers explain very little

to no variation in the magnitude or duration of bNCP (Fig S4). In contrast, coastal and coastal polynya Antarctic sea ice blooms have been shown to be primarily light limited (Joy-Warren et al., 2019; Park et al., 2017), suggesting different mechanisms may control primary and net community production in the SSIZ and in ice impacted coastal environments.

Drivers of higher daily NCP under actively retreating sea ice

Iron is known to limit phytoplankton growth in the Southern Ocean and iron from sea ice melt has previously been proposed to fuel SSIZ blooms (Croot et al., 2004; Delphine Lannuzel et al., 2008). Iron in sea ice is an order of magnitude greater than in surface waters, such that sea ice melt acts as a short-lived iron source (D. Lannuzel et al., 2016) and phytoplankton growth in the sea ice impacted Southern Ocean is strongly stimulated by additional iron (Alderkamp et al., 2019; Viljoen et al., 2018; Vives et al., 2022). Both grazing pressure and Fe limitation are thought to increase through the bloom season in the SSIZ (Moreau et al., 2020). In the present study, higher daily NCP rates occur while sea ice is still melting relative to the open water period, which leads to the majority of bNCP taking place under partial sea ice cover. The higher under-ice NCP is consistent with sea ice melt supplying micronutrients to the upper ocean and stimulating phytoplankton growth, which then decreases after total sea ice retreat.

Declining NCP rates as the season progresses (Fig. 3) may also result from increased grazing and/or shifts in phytoplankton community composition. Krill are effective grazers of phytoplankton blooms following sea ice retreat and have been observed to diminish phytoplankton populations within hours (Granĺi et al., 1993; Lancelot et al., 1991; Mengesha et al., 1998) and can significantly control NCP (Ishii et al., 2002). Community composition shifts linked to the sea ice environment have been shown to explain a high portion of variability in NCP in the West Antarctic

239 Peninsula, with more diverse plankton communities and higher NCP found when sea ice
240 concentration was higher during the summer sampling month (Lin et al., 2021). Iron limitation,
241 grazing, and community composition may all interact to drive the observed decrease in NCP
242 following total sea ice retreat. Phytoplankton communities are observed to shift from *Phaeocystis*
243 *Antarctica* to diatom communities throughout the season in response to increasing iron limitation
244 (Ryan-Keogh & Smith, 2021; Wright & van den Enden, 2000), while krill have been shown to
245 more effectively graze diatoms than and selectively graze diatoms over *Phaeocystis* (Davidson et
246 al., 2010; Haberman et al., 2003). Ecological modeling work suggests that the seasonal shift of
247 *Phaeocystis* and diatoms south of 60°S is controlled by temperature and iron, and the relative
248 importance of each to carbon cycling is also determined by biomass loss rates (Nissen & Vogt,
249 2020).
250
251 *Bloom NCP magnitude variability*
252 In addition to higher daily NCP rates during active sea ice retreat at a given location in the
253 SSIZ, estimated bNCP is higher when sea ice breaks up earlier relative to when sea ice breaks up
254 later in the year (Figs. 3c & 4a). This relationship cannot be primarily explained by a difference in
255 available light, as daily NCP rates are relatively higher even while estimated light is lower when
256 sea ice breaks up earlier in the year (Fig. 4b). We postulate that increased daily NCP associated
257 with anomalously early sea ice breakup could be due a greater lag between initial phytoplankton
258 biomass increases and grazer (predominately krill) biomass increases when sea ice breaks up
259 earlier in the year. Later sea ice breakup may reduce the lag, if zooplankton follow the sea ice
260 southward, which is consistent with observations of high krill abundances near the sea ice edge in

January and February, and southward krill migration over the season in the North Antarctic Peninsula (Brierley et al., 2022; Loeb & Santora, 2015).

The highest estimated bNCP (> 3.5 mol C m^{-2} $bloom^{-1}$) occurs in two regions; near Maud Rise and east of the Antarctic Peninsula (Fig. 1). Models of iron distribution within the Southern Ocean SSIZ and available in situ dissolved iron data (Laufkötter et al., 2018; Person et al., 2021; Tagliabue et al., 2012) indicate relatively high iron near the Eastern Antarctic peninsula. Flow topography interactions can enhance upwelling of deep waters throughout the Southern Ocean (Tamsitt et al., 2017) and specifically near Maud Rise (Bersch et al., 1992), and anomalous deep mixing has been observed near Maud Rise in 2016 and 2017 prior to the opening of open ocean polynyas (Campbell et al., 2019). This topographic-induced mixing could result in additional iron supply to support the highest bNCP values.

Spatial or interannual differences in micronutrient supply from sea ice melt may additionally explain some of the variance in bNCP, but this is currently difficult to assess as the dynamics and spatiotemporal variability of iron supply from melting sea ice are still not well constrained. Furthermore, we did not evaluate how the upper ocean processes that result in anomalously early sea ice break up or iceberg production could otherwise impact iron fertilization and subsequently bNCP. New proxies for iron limitation have been developed in the pelagic Southern Ocean (Schallenberg et al., 2022) and the coastal Ross Sea (Ryan-Keogh & Smith, 2021) and the addition of radiometers on under ice floats could allow for investigation of spatio-temporal patterns of iron limitation throughout the SSIZ.

Estimates of NCP or carbon export in the SSIZ that use NPP derived from satellite ocean color (~1-1.5 mol C m^{-2} yr^{-1}) (L. Arteaga et al., 2018; Li et al., 2021) are lower than estimates in this study. The fact that the majority (64%) of NCP associated with the SSIZ blooms occurs before

sea ice retreat is complete, suggests that estimates of NCP relying solely on satellite observations miss a significant portion of SSIZ bNCP and may not adequately capture spatial or temporal variations in NCP in the SSIZ. This is consistent with a prior modeling study that found that spring blooms began when SIC fell below 90% coverage and under ice NPP accounted for two thirds of the NPP in the marginal ice zone (MIZ, a subset of the SSIZ with actively retreating sea ice (Taylor et al., 2013a). These modeled under ice blooms yielded higher estimates of MIZ contribution to total Southern Ocean NPP south of 30°S (15%) than estimates from satellite ocean color observations (~4%) (Arrigo et al., 2008; Moore & Abbott, 2000; Taylor et al., 2013a). In the Southern Ocean south of 50°S, higher carbon export is estimated from inverse modeling and spring/summer climatological nitrate budgets relative to satellite derived methods, which could in part be in part explained by carbon export prior to full sea ice retreat (Maccready & Quay, 2001; Schlitzer, 2002). The estimates of NCP in this study focus solely on the bloom period and are therefore comparable in timing to satellite-based NCP estimates. The amount of organic carbon respired in winter should to be assessed in future work, as annual NCP estimated from one float in the Ross Sea indicated a near balance between positive spring bloom NCP offset by subsequent winter remineralization (Briggs et al., 2018).

Conclusions

The recent availability of under ice observations throughout the SSIZ has enabled examination of timing, mechanisms of bloom onset, and NCP associated with SSIZ blooms. By constraining the onset of biological production with nutrient data and matching this timing to estimates of sea ice breakup we find that biological production resulting in significant nutrient and carbon uptake in surface waters is not observed prior to initial sea ice breakup regardless of latitude

or incoming surface radiation. NCP estimates reveal that the majority of bNCP occurs as sea ice is actively melting, and the highest bNCP occurs in regions with potentially increased micronutrient delivery due to topographic features. This provides the first in-situ evidence that the SSIZ may contribute a far larger proportion of total Southern Ocean carbon export than had previously been observed, consistent with a few modeling studies.

The onset of phytoplankton biomass increase and nutrient drawdown occurs as sea ice first breaks up (~October), considerably before blooms have previously been observed by satellite ocean color and field surveys (~Jan-Feb). The lack of correlation between higher bNCP and cumulative light availability or duration of a shallow mixed layer provides new insight suggesting micronutrient availability, community composition, and/or grazing pressure are more important factors influencing SSIZ blooms and associated carbon export. The timing of sea ice breakup can explain a portion of the overall variance in total bNCP, which we suggest may result from earlier sea ice breakup leading to greater decoupling of phytoplankton growth and grazing loss. Our results indicate that future changes in sea ice seasonality, consolidation, and extent will all affect the timing and magnitude of SSIZ phytoplankton blooms and biogeochemistry, yet these changes are not likely to be predicted based on changes in light availability alone.

Open Research: Data and Code Availability

Float data used was downloaded from the SOCCOM project. The May 2021 quarterly snapshot dataset is used in this analysis and is available at doi.org/10.6075/J0T43SZG.

Mean surface downward short-wave radiation flux was downloaded from the Copernicus Climate Change Service (C3S) Climate Data Store https://doi.org/10.24381/cds.f17050d7 (Hersbach et al., 2020). The results contain modified Copernicus Climate Change Service

information 2020. Neither the European Commission nor ECMWF is responsible for any use that may be made of the Copernicus information or data it contains.

NOAA/NSIDC Climate Data Record of Passive Microwave Sea Ice Concentration, Version 4 (G02202) is available for download at https://doi.org/10.7265/efmz-2t65.

The International Bathymetric Chart of the Southern Ocean v2 digital bathymetric model is available for download at https://doi.org/10.1594/PANGAEA.937574.

Code used for the analysis is available for download at https://doi.org/10.5281/zenodo.7192130.

Author Contributions

S. McClish conducted the data analysis and writing of the manuscript. S. Bushinsky contributed to the data analysis and manuscript preparation.

Acknowledgements

S. McClish was supported by a Future Investigators in NASA Earth and Space Science and Technology (FINESST) award 80NSSC21K1641 and a NASA grant NNX17AI73G. S. Bushinsky was supported by NASA grants NNX17AI73G and 80NSSC22K0156.

Profiling float data were collected and made freely available by the Southern Ocean Carbon and Climate Observations and Modeling (SOCCOM) Project funded by the National Science Foundation, Division of Polar Programs (NSF PLR -1425989 and OPP-1936222), supplemented by NASA, and by the International Argo Program and the NOAA programs that contribute to it. (http://www.argo.ucsd.edu(link is external), http://argo.jcommops.org(link is external)). The Argo Program is part of the Global Ocean Observing System.

References

354 Ardyna, M., Claustre, H., Sallée, J. B., D'Ovidio, F., Gentili, B., van Dijken, G., et al. (2017).
355 Delineating environmental control of phytoplankton biomass and phenology in the Southern
356 Ocean. *Geophysical Research Letters*, *44*(10), 5016–5024.
357 https://doi.org/10.1002/2016GL072428
358 Arrigo, K. R., van Dijken, G. L., & Bushinsky, S. (2008). Primary production in the Southern
359 Ocean, 1997-2006. *Journal of Geophysical Research*, *113*(C08004),
360 doi:10.1029/2007JC004551. https://doi.org/10.1029/2007JC004551
361 Arteaga, L., Haëntjens, N., Boss, E., Johnson, K. S., & Sarmiento, J. L. (2018). Assessment of
362 Export Efficiency Equations in the Southern Ocean Applied to Satellite-Based Net Primary
363 Production. *Journal of Geophysical Research: Oceans*, *123*(4), 2945–2964.
364 https://doi.org/10.1002/2018JC013787
365 Arteaga, L. A., Pahlow, M., Bushinsky, S. M., & Sarmiento, J. L. (2019). Nutrient Controls on
366 Export Production in the Southern Ocean. *Global Biogeochemical Cycles*, *33*(8), 942–956.
367 https://doi.org/10.1029/2019GB006236
368 Arteaga, L. A., Boss, E., Behrenfeld, M. J., Westberry, T. K., & Sarmiento, J. L. (2020).
369 Seasonal modulation of phytoplankton biomass in the Southern Ocean. *Nature*
370 *Communications*. https://doi.org/10.1038/s41467-020-19157-2
371 Assmy, P., Fernández-Méndez, M., Duarte, P., Meyer, A., Randelhoff, A., Mundy, C. J., et al.
372 (2017). Leads in Arctic pack ice enable early phytoplankton blooms below snow-covered
373 sea ice. *Scientific Reports*, *7*(September 2016), 1–9. https://doi.org/10.1038/srep40850
374 von Berg, L., Prend, C. J., Campbell, E. C., Mazloff, M. R., Talley, L. D., & Gille, S. T. (2020).
375 Weddell Sea Phytoplankton Blooms Modulated by Sea Ice Variability and Polynya
376 Formation. *Geophysical Research Letters*, *47*(11), 1–12.
377 https://doi.org/10.1029/2020GL087954
378 Bersch, M., Becker, G. A., Frey, H., & Koltermann, K. P. (1992). Topographic effects of the
379 Maud Rise on the stratification and circulation of the Weddell Gyre. *Deep Sea Research*
380 *Part A, Oceanographic Research Papers*, *39*(2), 303–331. https://doi.org/10.1016/0198-
381 0149(92)90111-6
382 Bisson, K. M., & Cael, B. B. (2021). How Are Under Ice Phytoplankton Related to Sea Ice in the
383 Southern Ocean? *Geophysical Research Letters*, *48*(21), 1–9.
384 https://doi.org/10.1029/2021gl095051
385 Brierley, A. S., Fernandes, P. G., Brandon, M. A., Armstrong, F., Millard, N. W., McPhail, S. D.,
386 et al. (2022). *Antarctic Krill Under Sea Ice:Elevated Abundance in aNarrow Band Just*
387 *South ofIce Edge*. *13. G. R. Sarson, Philos. Trans. R. Soc. London Ser. A* (Vol. 24).
388 Academic Press. Retrieved from https://www.science.org
389 Briggs, E. M., Martz, T. R., Talley, L. D., Mazloff, M. R., & Johnson, K. S. (2018). Physical and
390 Biological Drivers of Biogeochemical Tracers Within the Seasonal Sea Ice Zone of the
391 Southern Ocean From Profiling Floats. *Journal of Geophysical Research: Oceans*, *123*(2),
392 746–758. https://doi.org/10.1002/2017JC012846
393 Buesseler, K. O., Barber, R. T., Dickson, M.-L., Hiscock, M. R., Moore, J. K., & Sambrotto, R.
394 (2003). The effect of marginal ice-edge dynamics on production and export in the Southern
395 Ocean along 1701W. *Deep-Sea Research II*, *50*, 579–603. https://doi.org/10.1016/S0967-
396 0645(02)00585-4
397 Bushinsky, S. M., & Emerson, S. R. (2018). Biological and physical controls on the oxygen
398 cycle in the Kuroshio Extension from an array of profiling floats. *Deep-Sea Research Part*

399 *I: Oceanographic Research Papers*, *141*(January), 51–70.
400 https://doi.org/10.1016/j.dsr.2018.09.005
401 Campbell, E. C., Wilson, E. A., Moore, G. W. K., Riser, S. C., Brayton, C. E., Mazloff, M. R., &
402 Talley, L. D. (2019). Antarctic offshore polynyas linked to Southern Hemisphere climate
403 anomalies. *Nature*, *570*(7761), 319–325. https://doi.org/10.1038/s41586-019-1294-0
404 Croot, P. L., Andersson, K., Öztürk, M., & Turner, D. R. (2004). The distribution and speciation
405 of iron along 6°E in the Southern Ocean. *Deep-Sea Research Part II: Topical Studies in*
406 *Oceanography*, *51*(22–24), 2857–2879. https://doi.org/10.1016/j.dsr2.2003.10.012
407 Davidson, A. T., Scott, F. J., Nash, G. v., Wright, S. W., & Raymond, B. (2010). Physical and
408 biological control of protistan community composition, distribution and abundance in the
409 seasonal ice zone of the Southern Ocean between 30 and 80°E. *Deep-Sea Research Part II:*
410 *Topical Studies in Oceanography*, *57*(9–10), 828–848.
411 https://doi.org/10.1016/j.dsr2.2009.02.011
412 Dorschel, B., Hehemann, L., Viquerat, S., Warnke, F., Dreutter, S., Tenberge, Y. S., et al.
413 (2022). The International Bathymetric Chart of the Southern Ocean Version 2. *Scientific*
414 *Data*, *9*(1). https://doi.org/10.1038/s41597-022-01366-7
415 Fitch, D. T., & Moore, J. K. (2007). Wind speed influence on phytoplankton bloom dynamics in
416 the Southern Ocean Marginal Ice Zone. *Journal of Geophysical Research: Oceans*, *112*(8),
417 1–13. https://doi.org/10.1029/2006JC004061
418 GranÍi, E., Granéli, W., Rabbani, M. M., Daugbjerg, N., Fransz, G., Roudy, J. C., & Alder, V. A.
419 (1993). The influence of copepod and krill grazing on the species composition of
420 phytoplankton communities from the Scotia Weddell sea - An experimental approach. *Polar*
421 *Biology*, *13*(3), 201–213. https://doi.org/10.1007/BF00238930
422 Haberman, K. L., Quetin, L. B., & Ross, R. M. (2003). Diet of the Antarctic krill (Euphausia
423 superba Dana): I. Comparisons of grazing on Phaeocystis antarctica (Karsten) and
424 Thalassiosira antarctica (Comber). *Journal of Experimental Marine Biology and Ecology*,
425 *283*(1–2), 79–95. https://doi.org/10.1016/S0022-0981(02)00466-5
426 Hague, M., & Vichi, M. (2020). Southern Ocean BGC-Argo Detect Under Ice Phytoplankton
427 Growth Before Sea Ice Retreat. *Biogeosciences Discussions*, 1–22.
428 https://doi.org/10.5194/bg-2020-257
429 Hersbach, H., Bell, B., Berrisford, P., Hirahara, S., Horányi, A., Muñoz-Sabater, J., et al. (2020).
430 The ERA5 global reanalysis. *Quarterly Journal of the Royal Meteorological Society*,
431 *146*(730), 1999–2049. https://doi.org/10.1002/qj.3803
432 Horvat, C., Bisson, K., Seabrook, S., Cristi, A., & Matthes, L. C. (2022). Evidence of
433 phytoplankton blooms under Antarctic sea ice. *Frontiers in Marine Science*, *9*.
434 https://doi.org/10.3389/fmars.2022.942799
435 Ishii, M., Inoue, H. Y., & Matsueda, H. (2002). Net community production in the marginal ice
436 zone and its importance for the variability of the oceanic pCO2 in the Southern Ocean south
437 of Australia. *Deep Sea Research Part II: Topical Studies in Oceanography*, *49*(9–10),
438 1691–1706. https://doi.org/10.1016/S0967-0645(02)00007-3
439 Johnson, K. S., Plant, J. N., Dunne, J. P., Talley, L. D., & Sarmiento, J. L. (2017). Annual nitrate
440 drawdown observed by SOCCOM profiling floats and the relationship to annual net
441 community production. *Journal of Geophysical Research: Oceans*, *122*(8), 6668–6683.
442 https://doi.org/10.1002/2017JC012839
443 Johnson, K. S., Plant, J. N., Coletti, L. J., Jannasch, H. W., Sakamoto, C. M., Riser, S. C., et al.
444 (2017). Biogeochemical sensor performance in the SOCCOM profiling float array. *Journal*

of Geophysical Research: Oceans, *122*(8), 6416–6436. https://doi.org/10.1002/2017JC012838

Joy-Warren, H. L., van Dijken, G. L., Alderkamp, A. C., Leventer, A., Lewis, K. M., Selz, V., et al. (2019). Light Is the Primary Driver of Early Season Phytoplankton Production Along the Western Antarctic Peninsula. *Journal of Geophysical Research: Oceans*, *124*(11), 7375–7399. https://doi.org/10.1029/2019JC015295

Lancelot, C., Billen, G., Veth, C., Becquevort, S., & Mathot, S. (1991). Modelling carbon cycling through phytoplankton and microbes in the Scotia—Weddell Sea area during sea ice retreat. *Marine Chemistry*, *35*(1–4), 305–324. https://doi.org/10.1016/S0304-4203(09)90024-X

Lannuzel, D., Vancoppenolle, M., Merwe, P. van der, Jong, J. de, Meiners, K. M., Nishioka, et al. (2016). Iron in sea ice: Review and new insights. https://doi.org/10.12952/journal.elementa.000130

Lannuzel, Delphine, Schoemann, V., de Jong, J., Chou, L., Delille, B., Becquevort, S., & Tison, J. L. (2008). Iron study during a time series in the western Weddell pack ice. *Marine Chemistry*, *108*(1–2), 85–95. https://doi.org/10.1016/j.marchem.2007.10.006

Laufkötter, C., Stern, A. A., John, J. G., Stock, C. A., & Dunne, J. P. (2018). Glacial Iron Sources Stimulate the Southern Ocean Carbon Cycle. *Geophysical Research Letters*, *45*(24), 13,377-13,385. https://doi.org/10.1029/2018GL079797

Li, Z., Lozier, M. S., & Cassar, N. (2021). Linking Southern Ocean Mixed-Layer Dynamics to Net Community Production on Various Timescales. *Journal of Geophysical Research: Oceans*, *126*(10), 1–14. https://doi.org/10.1029/2021JC017537

Lin, Y., Moreno, C., Marchetti, A., Ducklow, H., Schofield, O., Delage, E., et al. (2021). Decline in plankton diversity and carbon flux with reduced sea ice extent along the Western Antarctic Peninsula. *Nature Communications*, *12*(1), 1–9. https://doi.org/10.1038/s41467-021-25235-w

Loeb, V. J., & Santora, J. A. (2015). Climate variability and spatiotemporal dynamics of five Southern Ocean krill species. *Progress in Oceanography*, *134*, 93–122. https://doi.org/10.1016/j.pocean.2015.01.002

Maccready, P., & Quay, P. (2001). *Biological export flux in the Southern Ocean estimated from a climatological nitrate budget*. *Deep-Sea Research II* (Vol. 48).

Mengesha, S., Dehairs, F., Fiala, M., Elskens, M., & Goeyens, L. (1998). Seasonal variation of phytoplankton community structure and nitrogen uptake regime in the Indian Sector of the Southern Ocean. *Polar Biology*, *20*(4), 259–272. https://doi.org/10.1007/s003000050302

Moore, J. K., & Abbott, M. R. (2000). Phytoplankton chlorophyll distributions and primary production in the Southern Ocean. *Journal of Geophysical Research: Oceans*, *105*(C12), 28709–28722. https://doi.org/10.1029/1999jc000043

Moreau, S., Boyd, P. W., & Strutton, P. G. (2020). Remote assessment of the fate of phytoplankton in the Southern Ocean sea-ice zone. *Nature Communications*, *11*(1). https://doi.org/10.1038/s41467-020-16931-0

Nissen, C., & Vogt, M. (2020). Factors controlling the competition between <i>Phaeocystis</i> and diatoms in the Southern Ocean. *Biogeosciences Discussions*, (January), 1–39.

Park, J., Kuzminov, F. I., Bailleul, B., Yang, E. J., Lee, S. H., Falkowski, P. G., & Gorbunov, M. Y. (2017). Light availability rather than Fe controls the magnitude of massive

phytoplankton bloom in the Amundsen Sea polynyas, Antarctica. *Limnology and Oceanography*, *62*(5), 2260–2276. https://doi.org/10.1002/lno.10565

Parkinson, C. L. (2019). A 40-y record reveals gradual Antarctic sea ice increases followed by decreases at rates far exceeding the rates seen in the Arctic. *Proceedings of the National Academy of Sciences of the United States of America*, *116*(29), 14414–14423. https://doi.org/10.1073/pnas.1906556116

Person, R., Vancoppenolle, M., Aumont, O., & Malsang, M. (2021). Continental and Sea Ice Iron Sources Fertilize the Southern Ocean in Synergy. *Geophysical Research Letters*, *48*(23), 1–9. https://doi.org/10.1029/2021GL094761

Ryan-Keogh, T. J., & Smith, W. O. (2021). Temporal patterns of iron limitation in the Ross Sea as determined from chlorophyll fluorescence. *Journal of Marine Systems*, *215*, 103500. https://doi.org/10.1016/j.jmarsys.2020.103500

Schallenberg, C., Strzepek, R. F., Bestley, S., Bozena, W., & Trull, and T. W. (2022). Iron limitation drives the globally extreme Fluorescence/Chlorophyll ratios of the Southern Ocean. *Geophysical Research Letters*, *49*(12). https://doi.org/doi: 10.1029/2021GL097616

Schlitzer, R. (2002). Carbon export fluxes in the Southern Ocean: Results from inverse modeling and comparison with satellite-based estimates. *Deep-Sea Research Part II: Topical Studies in Oceanography*, *49*(9–10), 1623–1644. https://doi.org/10.1016/S0967-0645(02)00004-8

Smith, W. O., & Nelson, D. M. (1986). Importance of ice edge phytoplankton production in the Southern Ocean. *Bioscience*, *36*(4), 251–257. https://doi.org/10.2307/1310215

Smith, Walker O., & Comiso, J. C. (2008). Influence of sea ice on primary production in the Southern Ocean: A satellite perspective. *Journal of Geophysical Research: Oceans*, *113*(5), 1–19. https://doi.org/10.1029/2007JC004251

Smith, Walker O., & Nelson, D. M. (1985). Phytoplankton bloom produced by a receding ice edge in the ross sea: Spatial coherence with the density field. *Science*, *227*(4683), 163–166. https://doi.org/10.1126/science.227.4683.163

Tagliabue, A., Mtshali, T., Aumont, O., Bowie, A. R., Klunder, M. B., Roychoudhury, A. N., & Swart, S. (2012). A global compilation of dissolved iron measurements: Focus on distributions and processes in the Southern Ocean. *Biogeosciences*, *9*(6), 2333–2349. https://doi.org/10.5194/bg-9-2333-2012

Tamsitt, V., Drake, H. F., Morrison, A. K., Talley, L. D., Dufour, C. O., Gray, A. R., et al. (2017). Spiraling pathways of global deep waters to the surface of the Southern Ocean. *Nature Communications*, *8*(1). https://doi.org/10.1038/s41467-017-00197-0

Taylor, M. H., Losch, M., & Bracher, A. (2013a). On the drivers of phytoplankton blooms in the Antarctic marginal ice zone: A modeling approach. *Journal of Geophysical Research: Oceans*, *118*(1), 63–75. https://doi.org/10.1029/2012JC008418

Taylor, M. H., Losch, M., & Bracher, A. (2013b). On the drivers of phytoplankton blooms in the Antarctic marginal ice zone: A modeling approach. *Journal of Geophysical Research: Oceans*, *118*(1), 63–75. https://doi.org/10.1029/2012JC008418

Uchida, T., Balwada, D., Abernathey, R., Prend, C. J., Boss, E., & Gille, S. T. (2019). Southern Ocean Phytoplankton Blooms Observed by Biogeochemical Floats. *Journal of Geophysical Research: Oceans*, *124*(11), 7328–7343. https://doi.org/10.1029/2019JC015355

Viljoen, J. J., Philibert, R., van Horsten, N., Mtshali, T., Roychoudhury, A. N., Thomalla, S., & Fietz, S. (2018). Phytoplankton response in growth, photophysiology and community structure to iron and light in the Polar Frontal Zone and Antarctic waters. *Deep-Sea*

Research Part I: Oceanographic Research Papers, *141*(May), 118–129. https://doi.org/10.1016/j.dsr.2018.09.006

Wang, J., Luo, H., Yang, Q., Liu, J., Yu, L., Shi, Q., & Han, B. (2022). An Unprecedented Record Low Antarctic Sea-ice Extent during Austral Summer 2022. *Advances in Atmospheric Sciences*. https://doi.org/10.1007/s00376-022-2087-1

Wright, S. W., & van den Enden, R. L. (2000). Phytoplankton community structure and stocks in the East Antarctic marginal ice zone (BROKE survey, January-March 1996) determined by CHEMTAX analysis of HPLC pigment signatures. *Deep-Sea Research Part II: Topical Studies in Oceanography*, *47*(12–13), 2363–2400. https://doi.org/10.1016/S0967-0645(00)00029-1

References From the Supporting Information

Arteaga, L. A., Pahlow, M., Bushinsky, S. M., & Sarmiento, J. L. (2019). Nutrient Controls on Export Production in the Southern Ocean. *Global Biogeochemical Cycles*, *33*(8), 942–956. https://doi.org/10.1029/2019GB006236

Behrenfeld, M. J., & Boss, E. S. (2018). Student's tutorial on bloom hypotheses in the context of phytoplankton annual cycles. *Global Change Biology*. Blackwell Publishing Ltd. https://doi.org/10.1111/gcb.13858

de Boyer Montégut, C. (2004). Mixed layer depth over the global ocean: An examination of profile data and a profile-based climatology. *Journal of Geophysical Research*, *109*(C12), C12003. https://doi.org/10.1029/2004JC002378

Britton, C. M., & Dodd, J. D. (1976). Relationships of photosynthetically active radiation and shortwave. *Agricultural Meteorology* (Vol. 17).

Castellani, G., Schaafsma, F. L., Arndt, S., Lange, B. A., Peeken, I., Ehrlich, J., et al. (2020). Large-Scale Variability of Physical and Biological Sea-Ice Properties in Polar Oceans. *Frontiers in Marine Science*, *7*(August), 1–22. https://doi.org/10.3389/fmars.2020.00536

Elipot, S., & Gille, S. T. (2009). *Ekman layers in the Southern Ocean: spectral models and observations, vertical viscosity and boundary layer depth*. *Ocean Sci* (Vol. 5). Retrieved from www.ocean-sci.net/5/115/2009/

Graff, J. R., Westberry, T. K., Milligan, A. J., Brown, M. B., Dall'Olmo, G., van Dongen-Vogels, V., et al. (2015). Analytical phytoplankton carbon measurements spanning diverse ecosystems. *Deep-Sea Research Part I: Oceanographic Research Papers*, *102*, 16–25. https://doi.org/10.1016/j.dsr.2015.04.006

Haëntjens, N., Boss, E., & Talley, L. D. (2017). Revisiting Ocean Color algorithms for chlorophyll a and particulate organic carbon in the Southern Ocean using biogeochemical floats. *Journal of Geophysical Research: Oceans*, *122*(8), 6583–6593. https://doi.org/10.1002/2017JC012844

Hedges, J. I., Baldock, J. A., Gélinas, Y., Lee, C., Peterson, M. L., & Wakeham, S. G. (2002). *The biochemical and elemental compositions of marine plankton: A NMR perspective* (pp. 47–63). https://doi.org/10.1016/S0304-4203(02)00009-9

Hersbach, H., Bell, B., Berrisford, P., Hirahara, S., Horányi, A., Muñoz-Sabater, J., et al. (2020). The ERA5 global reanalysis. *Quarterly Journal of the Royal Meteorological Society*, *146*(730), 1999–2049. https://doi.org/10.1002/qj.3803

Ishii, M., Inoue, H. Y., & Matsueda, H. (2002). Net community production in the marginal ice zone and its importance for the variability of the oceanic pCO2 in the Southern Ocean south of Australia. *Deep Sea Research Part II: Topical Studies in Oceanography*, *49*(9–10), 1691–1706. https://doi.org/10.1016/S0967-0645(02)00007-3

Maurer, T. L., Plant, J. N., & Johnson, K. S. (2021). Delayed-Mode Quality Control of Oxygen, Nitrate, and pH Data on SOCCOM Biogeochemical Profiling Floats. *Frontiers in Marine Science*, *8*. https://doi.org/10.3389/fmars.2021.683207

Meier, W. N. , F. F. A. K. W. and J. S. S. (2021). NOAA/NSIDC Climate Data Record of Passive Microwave Sea Ice Concentration, Version 4 . Boulder, Colorado USA: National Snow and Ice Data Center.

Morel, A., Huot, Y., Gentili, B., Werdell, P. J., Hooker, S. B., & Franz, B. A. (2007). Examining the consistency of products derived from various ocean color sensors in open ocean (Case 1) waters in the perspective of a multi-sensor approach, *111*, 69–88. https://doi.org/10.1016/j.rse.2007.03.012

Papadimitriou, S., Kennedy, H., Norman, L., Kennedy, D. P., Dieckmann, G. S., & Thomas, D. N. (2012). The effect of biological activity, CaCO3 mineral dynamics, and CO2 degassing in the inorganic carbon cycle in sea ice in late winter-early spring in the Weddell Sea, Antarctica. *Journal of Geophysical Research: Oceans*, *117*(8), 1–12. https://doi.org/10.1029/2012JC008058

Verdy, A., & Mazloff, M. R. (2017). A data assimilating model for estimating Southern Ocean biogeochemistry. *Journal of Geophysical Research: Oceans*, *122*(9), 6968–6988. https://doi.org/10.1002/2016JC012650

Westberry, T., Behrenfeld, M. J., Siegel, D. A., & Boss, E. (2008). Carbon-based primary productivity modeling with vertically resolved photoacclimation. *Global Biogeochemical Cycles*, *22*(2). https://doi.org/10.1029/2007GB003078

Figure 1. **Mean float positions during spring bloom and associated net community production**. Ocean bathymetry (International Bathymetric chart of the Southern Ocean (IBSCO) version 2(Dorschel et al., 2022) overlayed with circular markers indicating float positions during spring nitrate minimum. Marker colors correspond to the magnitude of bNCP calculated from integrated upper ocean nitrate changes during each spring bloom.

Figure 2. Seasonal relationships between mixed layer properties and sea ice. Example float (WMO 5904471) winter to summer timeseries with mixed layer mean oxygen (orange), nitrate (red), phytoplankton carbon (blue), and chlorophyll (green) concentrations **(a.)** and mixed layer mean salinity, mixed layer depth, mixed layer median light **(b.)** with satellite SIC in shaded blue for both (SIC scale on bottom panel only). Symbols indicate the day of $GI_{Chl,Cp}$ or when nitrate, oxygen, or salinity thresholds are exceeded. **(c.)** Relationships between date of sea ice breakup relative to nitrate decrease and GI_{Cp} date. The day of year of nitrate decrease (red circles) and GI_{Cp} (blue triangles) vs. sea ice breakup day for all 64 float seasons analyzed. Colored lines indicate 20-day bin means ± 1 standard deviation. Symbols lying above the solid gold 1:1 line in the unshaded region indicate mixed layer nitrate decrease and GI_{Cp} after sea ice breakup.

Figure 3. Relationship between calculated NCP and sea ice cover. **a)** Average cumulative fraction of total bNCP for all floats (solid line) with respect to total sea ice retreat (dashed vertical

625 line) and ± 1 std deviation (shaded region). **b)** Probability histogram of daily NCP rates 50 days
626 before (green) and 50 days after (pink) total sea ice retreat date.
627

628 **Figure 4. Relationship between NCP and timing of sea ice breakup.** (**a.)** bNCP is negatively
629 correlated (red line, $P<.001$) with date of sea ice breakup. (**b.)** Differences between 10-day binned
630 mean daily NCP (purple line) and light availability (blue line) for early sea ice breakup and late
631 sea ice breakup observations (before mid-October, day 290) minus late (after early November, day
632 310). Floats with observations of early sea ice breakup had higher daily NCP prior to total sea ice
633 retreat despite lower light availability prior to total sea ice retreat.
634

Geophysical Research Letters

Supporting Information for

Majority of Southern Ocean seasonal sea ice bloom net community production precedes total ice retreat

Shannon McClish* and Seth M. Bushinsky

Department of Oceanography, School of Ocean and Earth Science and Technology, University of Hawai‘i at Mānoa, Honolulu, HI

Contents of this file

Text S1. Float Data

Water column biogeochemical measurements of under-ice and recently ice-free waters are from profiling floats deployed through the Southern Ocean Carbon and Climate Observation and Modeling (SOCCOM) project (Johnson, Plant, Coletti, et al., 2017) (May 2021 data snapshot). Quality controlled data from float conductivity-temperature-depth (CTD), chlorophyll fluorescence, pH, particulate backscatter, nitrate, and oxygen sensors were used and detailed quality control and processing methods are described in (Johnson, Plant, Coletti, et al., 2017; Maurer et al., 2021). Reported chlorophyll concentrations are derived from float fluorescence measurements corrected for non-photochemical quenching and adjusted based on an empirical fit to high-performance liquid chromatography (HPLC) measurements from samples taken during SOCCOM float deployments (Johnson, Plant, Coletti, et al., 2017).

Phytoplankton carbon is derived from float measured particulate backscatter ($b_{bp}(700)$):

$$POC = 3.12 \times 10^4 \ (\pm 2.47 \times 10^3) \times b_{bp}(700) + 3.0 \ (\pm 6.8) \qquad (1)$$

$$C_P = 0.19 \times POC \pm 8.7, \quad (2)$$

where POC is particulate organic carbon (mg C m^{-3}) (Haëntjens et al., 2017; Johnson, Plant, Coletti, et al., 2017) and C_P is phytoplankton carbon (mg C m^{-3}) (Graff et al., 2015).

Float data spans from July 2015 to March 2021, totaling 64 float years from 31 floats, and is broadly distributed throughout the Southern Ocean from approximately 55°S to 70°S (Fig. 1, Table S1). Any float timeseries that had more than one consecutive missing profile during the winter to summer period for any of the variables was removed from analysis.

Text S2. Light and Sea Ice Concentration

Float position estimates during the winter when the float remains under ice are linear interpolations between the last profile prior to sea ice cover and the first profile post sea ice retreat. Sea ice concentration (SIC) from NSDIC/NOAA Climate Data Record of Passive Microwave Sea Ice Concentration (Meier, 2021) and incident shortwave radiative flux from the ERA5 reanalysis (Hersbach et al., 2020) were matched to interpolated float tracks. Float data was included in the analysis if the float was under ice with satellite SIC >80% for at least one month of the year and if both the winter nitrate maximum and spring nitrate minimum were observed. After sea ice breakup, SIC is used to determine day of total sea ice retreat, defined herein as the first day of sea ice free conditions at the float location. One float season (WMO 5904859, 2017-18) never reaches 0% SIC, so the sea ice minimum day is used instead. Mixed layer depth is calculated based on a density threshold of 0.03 kg m^{-3} from 10 m or the shallowest measured depth for under-ice floats following (de Boyer Montégut, 2004). Mixed layer median light (I_g) is estimated as:

$$I_g = I_0 e^{-K_{PAR} \cdot \frac{MLD}{2}}, \quad (3)$$

where PAR at the surface (I_0) is estimated from 2.3*incident shortwave radiative flux at the surface (Britton & Dodd, 1976; Westberry et al., 2008). The diffuse attenuation coefficient of PAR (K_{PAR}) was estimated from (Morel et al., 2007):

$$K_{PAR} = 0.0864 + 0.884 \times K_{490} - 0.00137 \times {K_{490}}^{-1}, \text{ when MLD} \leq (K_{490})^{-1} \text{ m}^{-1} \quad (4)$$

$$K_{PAR} = 0.0665 + 0.874 \times K_{490} - 0.00121 \times {K_{490}}^{-1}, \text{ when MLD} > (K_{490})^{-1} \text{ m}^{-1}, \quad (5)$$

where K_{490}, the diffuse attenuation coefficient at 490nm, was derived from float estimated chlorophyll following (Morel et al., 2007):

$$K_{490} = 0.0166 + 0.0742\ Chl^{0.68955}. \quad (6)$$

I_g is adjusted for sea ice cover assuming a 10% transmittance through sea ice which falls within the range of available Southern Ocean transmittance observations (Castellani et al., 2020)

Text S3. Calculation of tracer timing thresholds

Float data were interpolated to a uniform daily timestep and 1m depth grid. Mixed layer property means, mixed layer depth, and depth integrated nitrate were smoothed with a 30-day running average. Nitrate was normalized to salinity to avoid sea ice melt biasing seasonal changes in nitrate due to biological processes, though this is a small adjustment (Papadimitriou et al., 2012).

The timing of the start of salinity decreases due to melt is identified as the day mixed layer salinity decreases by 0.015 from the winter maximum and continues to decrease to the minimum in spring. The satellite SIC threshold is identified when satellite SIC decreases by 2.5% from its maximum. The 0.015 salinity threshold was chosen to be comparable to the SIC threshold based on the mean slope of the linear regressions of satellite SIC and mixed layer mean salinity for each float as SIC decreases to 60% (Fig. S2, SIC vs mixed layer salinity).

The timing of initial sea ice breakup is estimated as the average of the three dates of mixed layer oxygen increase past threshold, mixed layer salinity decrease past threshold, and float matched SIC decrease past the threshold. Oxygen concentrations are strongly influenced by sea ice cover, which limits the exchange between the surface ocean and atmosphere, such that upwelled deep waters that are low in oxygen remain strongly undersaturated in the winter during maximum sea ice cover. Differences in sea ice breakup timing and melt estimated from salinity, satellite-derived SIC, or oxygen can be due to the uncertainty of float position under ice affecting satellite SIC to float matchups, uncertainties in satellite-derived SIC, a potential decoupling of freshening and sea ice cover due to melting and advection of sea ice, or increases in oxygen concentrations due to horizontal gradients and advection. However, there is good agreement between the timing of mixed layer oxygen increase, salinity decrease, and a decrease in sea ice concentration on the seasonal timescale of interest (Fig. S1). Estimating initial sea ice breakup from the average of all three proxies is done to minimize the impact of the particular uncertainties for each individual proxy.

Start of nitrate drawdown is determined when mean mixed layer nitrate concentrations drop below the winter maximum (mean of two highest values) minus 0.2 μmol kg^{-1} [NO_3^-]. The oxygen threshold calculated from the 0.2 μmol kg^{-1} nitrate concentration multiplied by an O:N stoichiometric ratio of 154/17 (Hedges et al., 2002). This was repeated using the mean July (winter) O:N ratio observed for each float and no difference in timing was found. Changes in mixed layer oxygen and nitrate can arise due to vertical or horizontal advection, entrainment, photosynthesis, or respiration, while oxygen is additionally exchanged with the atmosphere. Setting the oxygen threshold from the nitrate threshold is done to evaluate if changes in oxygen are driven by biology,

and therefore accompanied by changes in nitrate, or decoupled from nitrate changes and due to openings in sea ice cover and exposure to the atmosphere.

Timing of seasonal changes in phytoplankton biomass is estimated by calculating phytoplankton growth initiation (GI). GI is defined as the point when the time derivative of either Chl or C_p exceeds the median time derivative computed for the growth period and has previously been used to infer bloom phenology in the Southern Ocean seasonal sea ice zone (Hague & Vichi, 2020). GI was calculated using both float-derived mean mixed layer and MLD integrated Chl and C_p concentrations to test for differences due to accumulation or dilution. GI estimates from the rate of change in depth integrated and mean mixed layer concentrations are similar for both chlorophyll and C_p, and we use GI estimated from mean mixed layer concentration in the analysis as the mixed layer is primarily shoaling during the winter to spring period of interest (Behrenfeld & Boss, 2018).

Growth initiation estimates occur by definition after the first occurrence of an increase in rates of change (bloom onset) used in previous SSIZ phenology studies (Arteaga et al., 2020; Uchida et al., 2019). Growth initiation was chosen over bloom onset because $d[C_{phyto}]/dt$ can be >0 throughout the winter, even though MLD integrated and mean mixed layer $[C_{phyto}]$ remains near zero and nitrate is stable or increasing, and is thus less suitable for discerning when phytoplankton production begins to significantly impact surface biogeochemistry.

Text S4. Net Community Production

Net community production was calculated from the seasonal drawdown of salinity-normalized nitrate integrated to the depth of the deepest winter mixed layer from the preceding winter. This integration depth is chosen to estimate the amount of carbon removed from surface in the spring that would not be re-entrained the following winter, and to include production occurring just below

the base of the mixed layer. Changes in in nitrate that result from vertical and horizontal advection or diffusion are not explicitly estimated due to difficulty in accurately parameterizing these fluxes under sea ice and thus introduce uncertainty into the NCP estimates. However, we estimated the contribution from these processes to be small compared to the magnitude of biological drawdown during this period, as described below. Estimating NCP to the base of the winter mixed layer avoids uncertainties arising from that sporadic mixing events below the spring/summer MLD not captured by the float 10-day sampling, and reduces the contribution of vertical advection because the winter mixed layer is deeper than estimates of Ekman depth in the SSIZ (Elipot & Gille, 2009). Bloom NCP is estimated from the maximum nitrate profile after the deepest winter mixing to the minimum nitrate profile that occur between July and the end of March for each float. On average, the MLD max occurs 54 days before a mixed layer nitrate decreases past the threshold, but for four bloom timeseries only (5906033-2020, 5374-2018, 5904855-2018, 5904468-2017), the maximum MLD occurs between 1-8 days after mixed layer nitrate concentrations decrease past the threshold, and so the absolute maximum winter value of nitrate is used as the start of the bNCP calculation instead. To assess potential uncertainties due to horizontal advection, we referenced the Biogeochemical Southern Ocean State Estimate (BSOSE) (Verdy & Mazloff, 2017) upper 150m nitrate budgets from [iteration 121, 2013-2016], which indicate horizontal advection is small (approximately 10-15%) compared to the biological signal during the productive season (not shown, available online at http://sose.ucsd.edu/). BSOSE assimilates observations from biogeochemical floats, shipboard data, and satellites estimates and maintains closed budgets to provide an estimate of Southern Ocean biogeochemistry, physics, and sea ice state which has been extensively validated. While individual float data-model misfits do exist, we reference only the effect of advective processes on nitrate within the model. Furthermore, the NCP estimates in this

study are of a similar magnitude as NCP from previous in-situ studies using a variety of different methods (Arteaga et al., 2019; Briggs et al., 2018; Ishii et al., 2002; Johnson, Plant, Dunne, et al., 2017; Lin et al., 2021). Together, these comparisons give good confidence that the nitrate drawdown approach used in the present study are accurate estimates of bloom NCP. The reported p-values (two sided) and coefficients of determination were calculated with the SciPy stats pearsonr function**.**

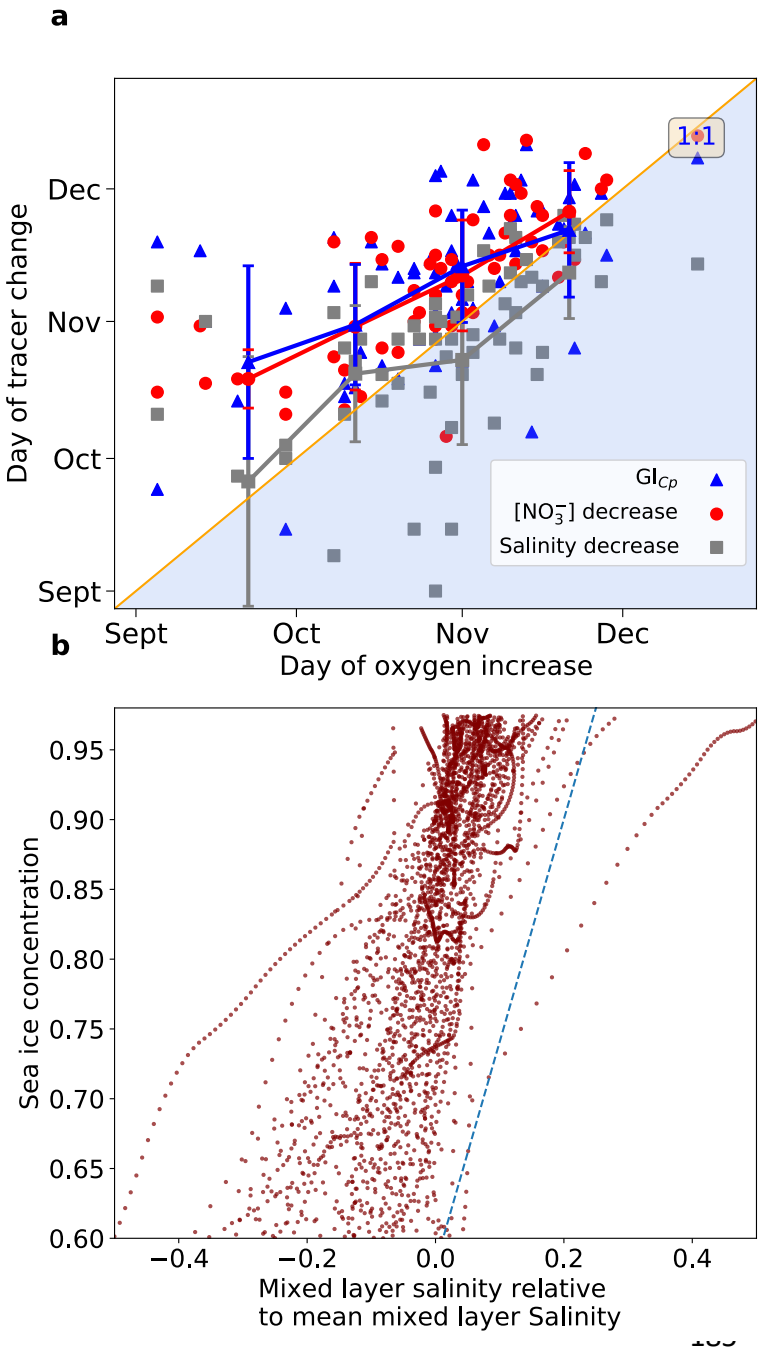

Figure S1. Rational for estimated timing of sea Ice break-up. A) Paper Figure 3 repeated with oxygen increase day instead of "Sea ice breakup day" on the x-axis and day of mean mixed layer nitrate decrease and GI_{Cp} vs float measured mean mixed layer salinity decrease day and on the y-axis. Twenty-day bin mean and standard deviations are shown by the error bars of the same color. Sea ice breakup used in analysis is the mean of the day of SIC decrease, day of salinity decrease and oxygen increase to indicate sea ice breakup. Oxygen increase and salinity decrease timing fall on or near the 1:1 line on average, while GICp and nitrate decrease follow (fall above 1:1 line) oxygen increase and salinity decrease.

B) Changes in mixed layer salinity relative to sea ice melt were assessed to determine comparable salinity and SIC thresholds. The mean mixed layer salinity (relative to mean salinity for clarity) is plotted vs satellite SIC during the period of initial SIC decrease to 60% SIC. The salinity threshold used in the analysis was determined from the mean slope of a linear regression line for each float mixed layer S vs. SIC which is 1.6 after outliers (25th and 75th quantiles) are removed. The mean slope used is indicated in the figure with the blue dashed line. This indicates an approx. ~.015 change in mixed layer salinity for the 2.5% SIC decrease threshold.

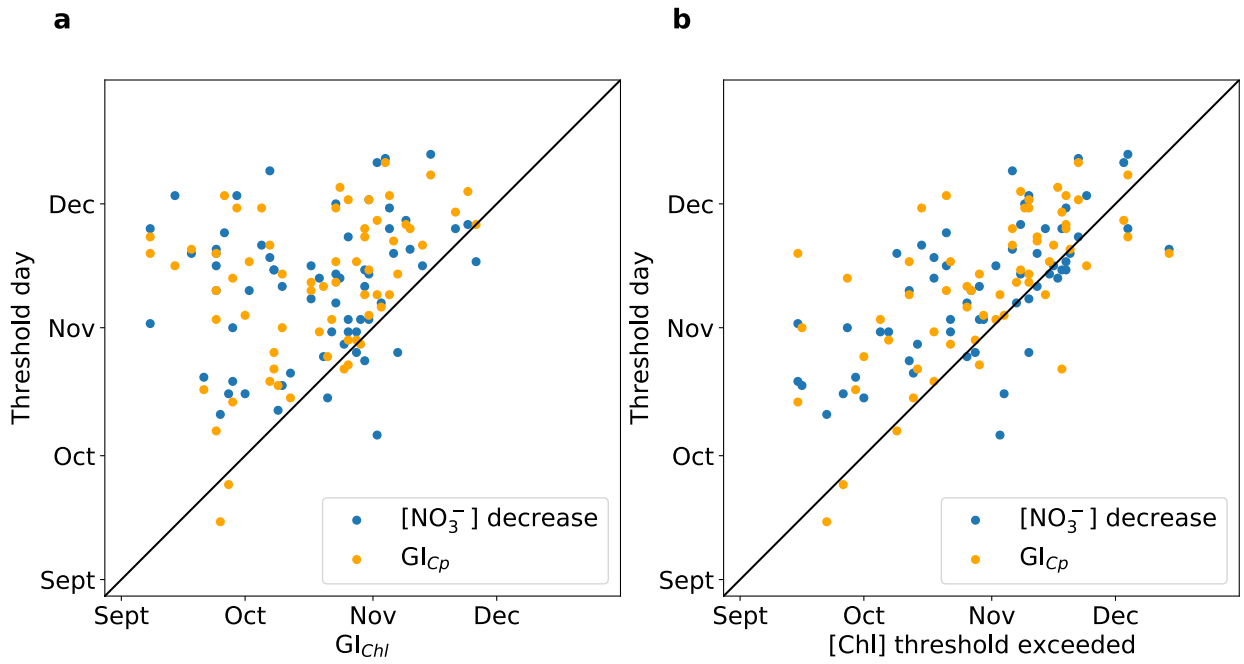

Figure S2. **Relationship between nitrate threshold and GI_{Cp} and two different chlorophyll-based growth initiation metrics**. a) Comparison of GI_{chl} vs timing of timing of nitrate decrease past the 0.2 µmol/kg threshold and GI_{Cp} (b) Comaprison of timing of chl exceeding 0.035mg/m^3 vs timing of nitrate decrease past 0.2 µmol/kg threshold and $GI_{Cp.}$ Estimation of growth intiation from the timing of an increase in the rate of mixed layer chlorphyll concentration was sensitive to small increases in chlorophyll (<.035mg/m^3) that were before an increase in Cp or nitrate concentration decrease, which both plot well above the 1:1 line on a). Earlier GI_{chl} was not consistent, but could occur months before, to within days of GI_{Cp} and nitrate decrease, making GI_{chl} not appropriate for determining when phytoplankton began to drawdown surface nutrients and carbon.

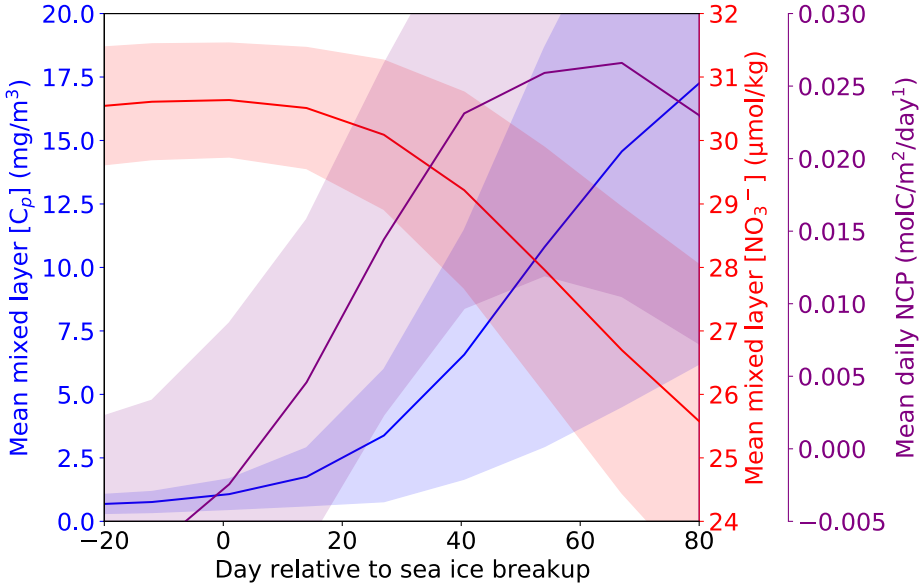

Figure S3. Comparison between temporal changes in mean mixed layer nitrate and C_{phyto} concentrations and daily NCP with respect to sea ice breakup. 10-day binned mean daily NCP (purple line), mean mixed layer nitrate (red line), mean mixed layer C-phyto (blue line) vs. day relative to sea ice breakup. Standard deviations shown by shaded area for each. Daily NCP > 0 after sea ice breakup, consistent with increases in phytoplankton carbon and mixed layer nitrate decrease.

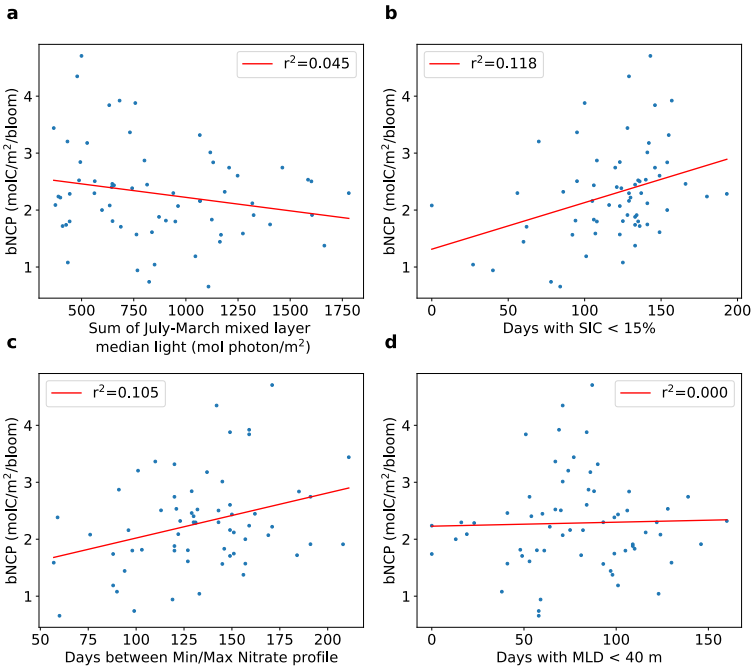

Figure S4. Light availability is not found to be primary factor influencing the magnitude of bNCP. Scatter plots and ordinary linear regression (red line) between bNCP and a) sum of mixed layer median light from July to end of March , b) days SIC < 15%, c) Days between min and max Nitrate profile (time over which bNCP is calculated), and d) days with a MLD <40m. The

respective *P*-values are a).091 b) .005, c).009, d) .817. bNCP shows a weak but significant relationship with the number of days with SIC < 15%, but this is confounded by the fact that earlier sea ice retreat will by definition lead to more days with SIC <15%. If this relationship were equal to or stronger than the bNCP vs. Sea ice breakup day (Fig. 5) it could have indicated that the primary factor controlling bNCP was duration of open water; however, this does not appear to be the case.

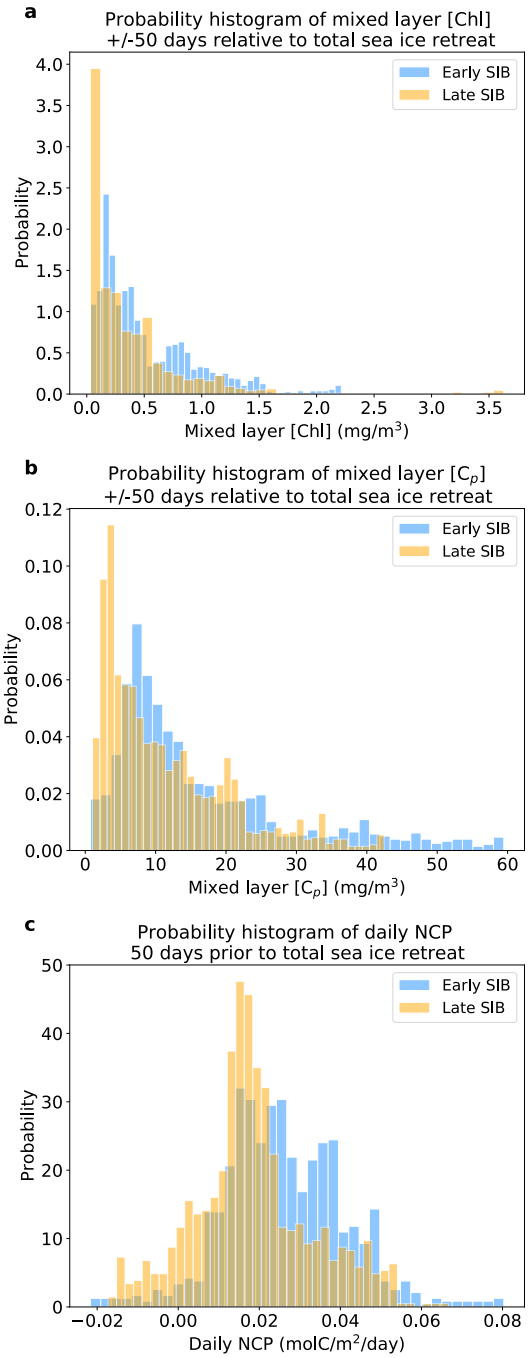

Figure S5. Higher daily NCP prior to total sea ice retreat and overall higher later winter/spring mixed layer chlorophyll and C_{phyto} concentrations for floats that observe early vs. late sea ice breakup. A) Daily NCP rates comparing occurrences of early (blue) and late (gold) sea ice breakup in the 50 days before complete sea ice retreat (open water day). B) Mean mixed layer chlorophyll and C) phytoplankton carbon (right) concentrations for the 50 days before and after open water day comparing early vs late SIB occurrences.

Table S1. WMO Float ID, year, mean float-season locations, bNCP, fraction bNCP before total sea ice retreat, and tracer timings for all float seasons analyzed.

Float WMO	Year[1]	Mean Latitude during bloom (°N)	Mean Longitude during bloom (°E)	Oxygen threshold (year day)	Sea Ice Breakup (year day)	Salinity threshold (year day)	Oxygen threshold (year day)	GI_{Cp} (year day)	GI_{Chl} (year day)	bNCP (mol C m^{-2} $bloom^{-1}$)
5904180	2015	-65.4	203.8	248	259	313	306	323	251	2.3
5904180	2016	-64.5	206.1	285	272.7	296	293	290	264	1.6
5904397	2015	-61.6	344.9	314	314.7	316	329	327	251	1.6
5904397	2016	-60.4	128.8	320	297.3	298	321	330	330	2.3
5904397	2017	-61.8	247.1	297	292	301	307	301	302	2
5904397	2018	-60.4	351.7	320	314.3	313	329	313	309	1.7
5904467	2015	-61	4.2	318	310	315	323	280	267	1.1
5904467	2016	-62.3	352.8	303	292	281	314	321	275	2.5
5904467	2017	-59.9	352.3	272	268	274	284	258	268	2.2
5904468	2015	-64.5	3.1	299	295.3	289	318	319	304	2.5
5904468	2016	-66.1	4.2	272	277.3	277	289	308	274	3
5904468	2017	-64.8	37.7	257	265.7	305	291	305	283	3.8
5904468	2018	-64.6	2.1	310	305	313	320	325	317	3.2
5904471	2015	-65.9	2.2	293	304.3	291	322	292	280	2.8
5904471	2016	-65.1	2.8	300	290	272	311	316	296	2.7
5904471	2017	-64.7	5.6	263	256.3	270	292	287	271	3.9
5904471	2018	-67.1	5.4	312	301	301	320	314	290	2.4
5904472	2015	-68.5	345.9	315	305.3	299	324	329	314	1.8
5904472	2016	-69.1	338.7	311	298.7	282	317	304	292	2.9
5904472	2017	-69.2	330.1	315	309.3	307	336	336	304	1.2

5904472	2018	-66.7	318.4	309	318.3	321	345	331	306	0.7
5904855	2018	-68.7	274.8	302	292.3	297	279	313	306	2.7
5904855	2019	-68.9	277	315	321.7	324	318	321	296	1.8
5904859	2017	-70.1	257.3	349	330	318	347	342	319	2.1
5905075	2017	-68.1	255.1	296	280.3	304	305	317	271	2.2
5905075	2018	-69.9	260.1	319	316.3	293	331	330	313	1
5905077	2017	-65.7	254.9	283	285.3	284	294	288	285	2.3
5905078	2017	-66.7	235.1	300	315.7	309	330	338	328	2.5
5905080	2018	-68.1	263.7	303	280	258	304	307	295	1.9
5905080	2019	-67.3	281	248	278.3	284	289	267	270	2.6
5905100	2017	-65.4	167.3	286	270.3	301	288	298	294	3.4
5905100	2018	-65	164.8	300	277.3	244	301	295	298	2.2
5905102	2017	-69.8	172.5	324	328.3	329	323	326	310	1.7
5905374	2018	-64.2	141.9	293	294	301	298	315	293	2.5
5905635	2018	-67.1	190	306	296.3	311	314	314	267	1.8
5905635	2019	-66.4	191	305	309.3	293	311	310	307	1.7
5905636	2018	-67	210.5	304	300.7	306	315	318	283	1.8
5905636	2019	-66.9	210.6	325	328.3	324	329	333	325	2.1
5905636	2020	-67	210.7	332	324.3	328	337	320	257	2.1
5905637	2018	-71.4	204.1	331	311	314	335	334	296	1.4
5905637	2019	-71.3	190.1	326	331.7	327	327	336	299	2.3
5905637	2020	-69	190.7	323	314	323	315	327	303	3.2
5905638	2018	-68.4	174.1	328	325.7	324	343	325	280	0.7
5905638	2019	-69.1	172.2	326	330	320	319	299	281	0.9
5905639	2018	-67.3	236.2	313	294.3	309	325	334	278	2.4
5905991	2019	-61.7	323.2	290	290.7	287	319	295	281	1.9
5905991	2020	-59.2	325.7	281	250.3	252	297	313	303	4.7
5905992	2019	-65.9	330.4	300	300	301	320	307	267	1.7
5905992	2020	-64.6	330.4	303	302.7	301	319	329	303	3.4

5905994	2019	-65.2	320.3	301	311	305	317	339	297	3.9
5905994	2020	-64.4	323.8	317	315.7	319	346	345	308	2.2
5905995	2019	-67	342	314	322	326	337	334	272	1.6
5905995	2020	-67.6	338.6	316	315.7	314	334	337	309	1.6
5905997	2019	-64.4	119.6	230	267.7	277	299	302	301	2.4
5905997	2020	-63.9	117.1	300	284.3	306	304	302	299	1.8
5905998	2020	-63.7	123.8	283	288.7	299	285	291	282	2.5
5906000	2019	-63.5	100.2	256	264	218	304	321	301	2.3
5906005	2019	-59.7	329.3	305	297.7	296	307	296	299	3.3
5906005	2020	-59.6	330.4	296	273.7	258	312	316	290	4.3
5906006	2019	-58.6	339.1	307	304	302	307	308	304	2.8
5906033	2019	-66.5	22.4	288	303.3	314	324	323	267	1.9
5906033	2020	-66.8	0	307	303.7	298	328	337	269	2.4
5906034	2019	-63	28.5	290	290.7	293	299	318	311	2.1
5906034	2020	-64.1	28	281	295.3	307	323	324	261	1.4

[1]Year corresponds to the winter/spring year for each bloom period.